Materials Advances

Accepted Manuscript

This article can be cited before page numbers have been issued, to do this please use: Y. Okuyama, R. Kawakami and K. Douzono, *Mater. Adv.*, 2026, DOI: 10.1039/D6MA00607H.

ROYAL SOCIETY OF CHEMISTRY

rsc.li/materials-advances

View Article Online
DOI: 10.1039/D6MA00607H

ARTICLE

Prediction and exploration of proton conductivity using machine learning in proton-conducting ceramics

Received 00th January 20xx,
Accepted 00th January 20xx

DOI: 10.1039/x0xx00000x

Yuji Okuyama,*[a] Renta Kawakami,[b] and Kota Douzono,[b]

Proton-conducting ceramic fuel cells, a type of solid-oxide fuel cell, are being considered for use at 300°C–600°C due to their electrolyte properties. Therefore, we used machine learning to identify new materials that exhibit high proton conductivity at low temperatures. We constructed a database comprising proton (726 data points from 76 perovskite-type oxide compositions) and hole conductivity data (738 data points from 103 perovskite-type oxide compositions). Using gradient boosting, we predicted proton conductivity based on various descriptors, including ionic radius and electronegativity. The structure of the virtual composition was perovskite-type (ABO3), and the host elements of the A and B sites were assumed to be Ba, Sr, and Ca and Co, Mn, Ni, and Fe, respectively. The additive elements of the B site were assumed to be Er, Gd, In, Lu, Ru, Sc, Y, and Yb. Hypothetical compositions, $BaMn_{(1-x)/2}Y_{(1-x)/2}In_xO_3$ (x = 0.1, 0.3, 0.5, 0.7), based on predicted high proton and low hole conductivities were synthesized using the liquid phase method. The isotope effect on electrical conductivity was confirmed at 800°C–400°C, using 1.9%H_2O (or D_2O)-1%O_2-Ar, and observed at low temperatures (400°C) for x = 0.3, 0.5, and 0.7. Therefore, $BaMn_{(1-x)/2}Y_{(1-x)/2}In_xO_3$ (x = 0.3, 0.5, 0.7) was found to be a proton conductor. However, the proton conductivity was found to be low, below the predicted value.

Introduction

Since the discovery of proton-conducting ceramics by Iwahara et al.[1] in 1980, there has been considerable research on their material development. Acceptor-doped $BaCeO_3$ and $BaZrO_3$ have been reported to exhibit proton conductivity exceeding 10^{-2} S cm^{-1} at temperatures over 600°C[2,3]. Recently, $BaZrO_3$, $BaSnO_3$, and $BTiO_3$ doped with Sc in high concentrations have been reported to exhibit high proton conductivity at temperatures of 300°C–400°C[4]. In the case of proton-conducting oxides, protons are generated by incorporating water vapor into the oxide crystal structure by filling oxide ion vacancies. existing as interstitial defects near oxygen ions. By hopping during thermal activation, they exhibit proton conductivity. Oxides that exhibit high proton conductivity at temperatures between 200°C and 400°C are attracting attention as fuel cell electrolytes for heavy-duty vehicles (HDVs).

This study also investigates the effects of the type and concentration, as well as the relationships of the added elements with crystal structures[5–23]. Perovskite-type oxides possess the most reported proton-conducting oxides. The following are examples for $SrCeO_3$[5], $SrZrO_3$[1], $BaCeO_3$[6,7], $BaZrO_3$[8], and $CaZrO_3$[9]. Additional compounds reported to exhibit proton conductivity include the following: II–IV perovskite oxides composed of divalent and tetravalent cations; III–III perovskite oxides composed of trivalent cations, such as $LaErO_3$[10], $LaScO_3$[11,12], and $LaYbO_3$[13]. Furthermore, proton conductivity is displayed in the I–V type compound $KTaO_3$, which is composed of monovalent and pentavalent cations[14]. Among non-perovskite crystal structures, proton conductivity has been observed in the following compounds: $La_2Zr_2O_7$ with a pyrochlore structure[15]; $LaPO_4$ with a monazite structure[16]; YPO_4 with a xenotime structure[17]; $LaNbO_4$ with a Ferguson structure[18]; Y_2O_3 with a C-rare-earth structure[19]; and αAl_2O_3 with a corundum structure[20,21]. Proton diffusion has been reported in oxides such as $MgAl_2O_4$ (with a spinel structure) and $LiTaO_3$ (with an ilmenite structure), where protons are not the primary charge carriers[22,23]. However, determining the effects of adding multiple elements, including the synergistic effects of co-addition, involves an enormous number of possible combinations of compositions. Experimentally discovering new materials under these conditions requires immense cost and time.

In recent years, the adoption of AI has been promoted across various industrial fields. In materials development, advances in machine-learning-based prediction technologies for material properties have demonstrated their usefulness in accelerating development. In the research and development of proton-conducting ceramics, the discovery of new materials has been achieved through machine-learning-based hydration prediction[24]. Furthermore, machine learning enables the prediction of crystal phases in proton-conducting ceramics[25].

[a] Department of Applied Chemistry, Faculty of Engineering, University of Miyazaki, 1-1 Gakuenkibanadai-nishi, Miyazaki 889-2192 Japan Email: okuyama@cc.miyazaki-u.ac.jp
[b] Department of Environmental Robotics, Mechanical Systems, and Informatics Course, Graduate School of Engineering, University of Miyazaki, 1-1 Gakuenkibanadai-nishi, Miyazaki 889-2192, Japan
Supplementary Information available: [details of any supplementary information available should be included here]. See DOI: 10.1039/x0xx00000x

View Article Online
DOI: 10.1039/D6MA00607H

In this study, a machine learning tool was constructed to predict proton conductivity in oxides. Additionally, new multi-element-substituted proton-conducting ceramics were explored. The prediction accuracy of the tool was verified using cross-validation and the relationship between material properties and descriptors was investigated. Furthermore, the impact of data quality and quantity on the prediction accuracy was clarified. The virtual composition's structure was assumed to be perovskite-type (ABO_3). The host elements for the virtual composition sites were assumed as follows: (i) virtual composition A site: Ba, Sr, and Ca and (ii) virtual composition B site: Co, Mn, Ni, and Fe (which are not typically used in proton conductors.) The additive elements of the B site were assumed to be Er, Gd, In, Lu, Ru, Sc, Y, and Yb as acceptor dopants. We synthesized the proton-conducting ceramics recommended by the model and evaluated their proton conductivity.

Results and discussion

Material selection via machine learning

Validation of machine learning models for proton conductivity We constructed a supervised machine learning model in which proton conductivity was the target variable and composition-dependent parameters were the descriptors (Figure S1). The supervised machine learning model used experimental proton conductivities from 76 compositions and 726 samples (Table S1). We chose $\log(\sigma_{proton})$ to emphasize the lower proton conductivity range as the target variable. The descriptors comprised 75 physical property values derived from electrolyte elemental information, including electronegativity, atomic density, atomic mass, ionic radius, melting point, and first ionization energy, as well as average ABO_3 compositions, average values for the A site, and average values for the B site. The descriptors were those previously reported for the prediction of hydration levels using machine learning[24].

Proton conductivity predictions were generated using three learning algorithms: gradient boosting, random forest, and AdaBoost regressors. The prediction accuracy and importance of each learning algorithm were calculated. The influence of the target variable on the prediction was then confirmed for gradient boosting regression, the learning algorithm with the highest prediction accuracy. In this study, we performed cross-validation for each composition using the Leave-One-Group-Out method. To evaluate prediction accuracy, we used the root-mean-square error (RMSE) for each composition, calculated from the predicted values obtained via cross-validation and the actual measured values. RMSE, the most common performance metric for regression models, was used as the indicator of prediction accuracy, as follows:

$$\mathrm{RMSE} = \sqrt{\frac{1}{n}\sum_{i=1}^{n}(y_i - \hat{y}_i)^2} \quad . \qquad (1)$$

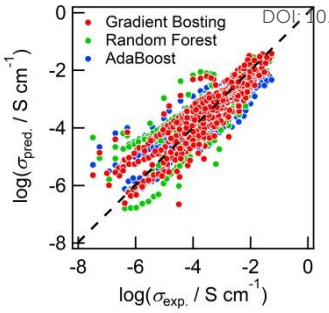

Figure 1 Cross-validation of proton conductivity for each learning algorithm

Table 1 Proton conductivity prediction accuracy for each machine learning model

Machine Learning Model	RMSE
Gradient boosting	0.48182
Random forest	0.56832
AdaBoost	0.57682

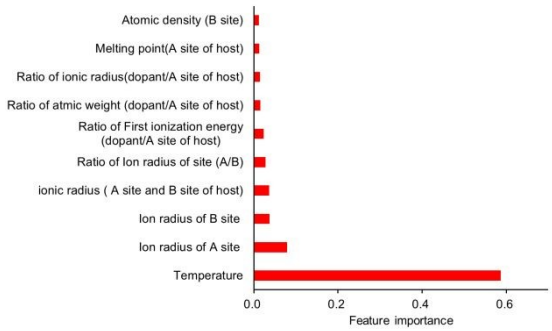

Figure 2 Feature importance for the prediction of proton conductivity using the gradient boosting model

As shown in Figure 1 and Table 1, the gradient boosting regressor produced the smallest RMSE and was therefore the most suitable learning model for predicting proton conductivity.

Figure 2 shows the top 10 descriptor importance values for the gradient boosting regression model predictions. As shown in Figure 2, temperature was the most important predictor, while ionic radius, first ionization energy, atomic weight, melting point, and atomic density of ABO_3 perovskite oxides influenced the predictions.

It was necessary to assess the impact of the database on the prediction accuracy. The predictions were performed on the following two datasets: (i) Dataset 1 comprises of proton conductivity of perovskite oxides composed of divalent and tetravalent cations (48 compositions, 493 samples) and (ii) Dataset 2 comprises of proton conductivity of perovskite oxides

View Article Online
DOI: 10.1039/D5MA00607H

composed of trivalent and trivalent cations (28 compositions, 233 samples).

Using these two datasets, we predicted the proton conductivity of perovskite oxides composed of (i) divalent and tetravalent cations and (ii) perovskite oxides composed of trivalent and trivalent cations. The cross-validation results of the two datasets are shown in Figure 3. As shown in Figure 3(a), the model trained on Dataset 1 achieved the highest prediction accuracy. Conversely, Figure 3(b) shows that the model trained on Dataset 2 exhibited significant discrepancies between predicted and measured proton conductivities for perovskite oxides composed of divalent and tetravalent cations. Figure 3(a) shows that high prediction accuracy was achieved for the proton conductivities of perovskite oxides composed of trivalent and trivalent cations. Moreover, the plot shows the predictions of proton conductivity for perovskite oxides composed of divalent and tetravalent cations based on data from the same. This is considered as an interpolation prediction for descriptors and proton conductivity. Additionally, Figure 3(a) predicts proton conductivities for perovskite oxides composed of trivalent and trivalent cations based on data from the same, suggesting interpolation-based prediction. Figures 3(a) and 3(b) predict perovskites with compositions different from the dataset; however, no decrease in prediction accuracy is evident in Figure 3(a). This is likely because the proton conductivity of perovskite oxides composed of divalent and tetravalent cations covers a broad range (~10^{-2}–10^{-7} S cm^{-2}). Since the dataset includes the proton conductivity range of perovskite oxides composed of trivalent and trivalent cations, which enablse interpolation prediction and thus avoids a decrease in prediction accuracy. Conversely, its proton conductivity covers a limited range (10^{-2} to 10^{-5} S cm^{-2}).This results in the inability to predict proton conductivities below 10^{-5} S cm^{2} for perovskite oxides composed of divalent and tetravalent cations, as displayed in Figure 3(b). This suggests that collecting diverse data for the target variables and descriptors in the database enables the prediction of proton conductivity across a wide range of compositions.

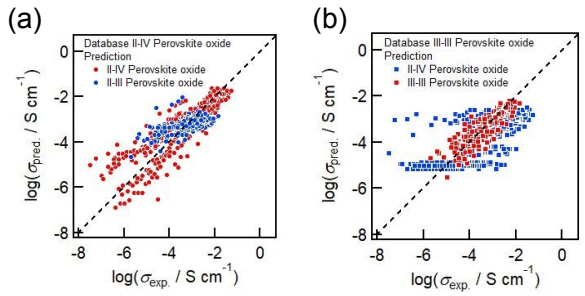

Figure 3 Cross-validation results based on two datasets

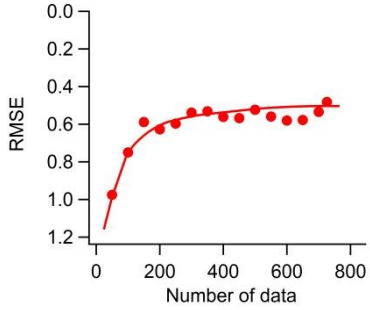

Figure 4 Data-number dependence of RMSE for the prediction of proton conductivity

To examine the impact of dataset size on prediction accuracy, the dependence of RMSE on the number of data points was investigated. As shown in Figure 4, the RMSE retains a constant for datasets with 150 or more data points. This study constructed a prediction model using 726 data points while ensuring sufficient data for accurate predictions.

Validation of machine learning models for hole conductivity We constructed a supervised learning model, with hole conductivity as the target variable and composition-dependent parameters as descriptors. The machine learning was performed using

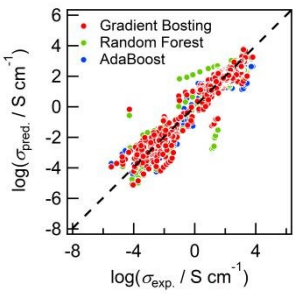

Figure 5 Cross-validation of hole conductivity for each machine learning model

Table 2 Effect of data variation on prediction accuracy

Dataset	Prediction	RMSE
II–IV type perovskite oxide	II–IV type perovskite oxide	0.62342
	II–-III type perovskite oxide	0.59294
III–III type perovskite oxide	II–IV type perovskite oxide	1.03668
	III–III type perovskite oxide	0.35584

Table 3 Prediction accuracy of hole conductivity for each machine learning model

Machine Learning Model	RMSE
Gradient boosting	0.5810
Random forest	0.6326
AdaBoost	0.5565

View Article Online
DOI: 10.1039/D6MA00607H

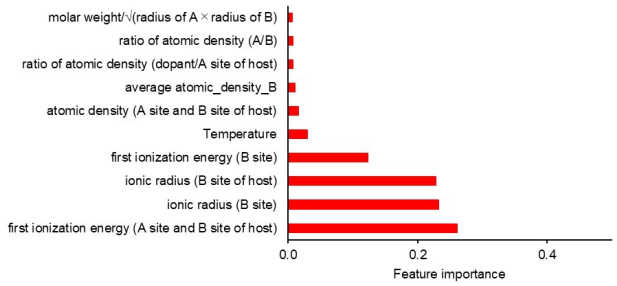

Figure 6 Data number dependence of RMSE for the prediction of hole conductivity

experimental hole conductivity values for 103 compositions and 738 samples (Table S2). We chose log(σ_{hole}) to emphasize the lower hole conductivity range as the target variable. The descriptors used for the prediction comprised 75 physical property values derived from elemental information, similar to those used to predict the proton conductivity.

Figure 5 and Table 3 show that AdaBoost produced the smallest RMSE and was therefore the most suitable learning model for predicting hole conductivity. The importance of descriptors for predicting proton conductivity in gradient boosting was demonstrated. Comparatively, Figure 6 shows the importance of descriptors in gradient boosting for predicting hole conductivity. Unlike proton conductivity, the first ionization energy is more important for predicting hole conductivity.

Prediction of proton and hole conductivity for virtual compositions The proton conductivity and hole conductivity of ABO_3 oxides with A site Ba, Sr, and Ca and B site Mn, Co, Fe, and Ni were predicted using machine learning. As shown in Figures 7(a) and (b), the predictions suggest that $BaMnO_3$ exhibits the highest proton conductivity and lowest hole conductivity as the matrix phase.

Furthermore, the effect of adding elements to $BaMnO_3$ on its proton conductivity was predicted. The effects of adding Gd, Y, Yb, In, and Sc as the first additive element on proton and hole conductivities were predicted using machine learning. As displayed in Figure 8, adding Y, Ru, or Sc was predicted to yield high proton conductivity. However, it was inferred that the hole conductivity could be suppressed by adding In, Er, Gd, or Lu. It was predicted that adding Y would effectively enhance proton conductivity, while adding In would effectively suppress hole conductivity. Since the Ba-Mn-Y-In-O system has been proposed as a candidate proton-conducting oxide, we predicted the proton and hole conductivities of $BaMn_{(1-x)/2}Y_{(1-x)/2}In_xO_3$. Figure 9 shows that the predicted proton conductivity did not reach 0.01 S/cm, but it exhibited relatively high proton conductivity. On the other hand, the hole conductivity exhibited a higher value than the proton conductivity, suggesting mixed conductivity. However, predictions of proton and hole

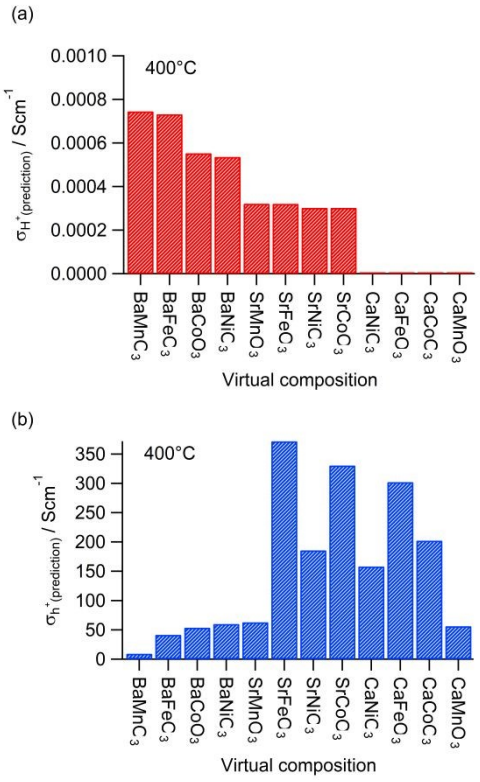

Figure 7 Prediction of the proton and electronic conductivities of the ABO_3 matrix. (a) Proton and (b) hole conductivity

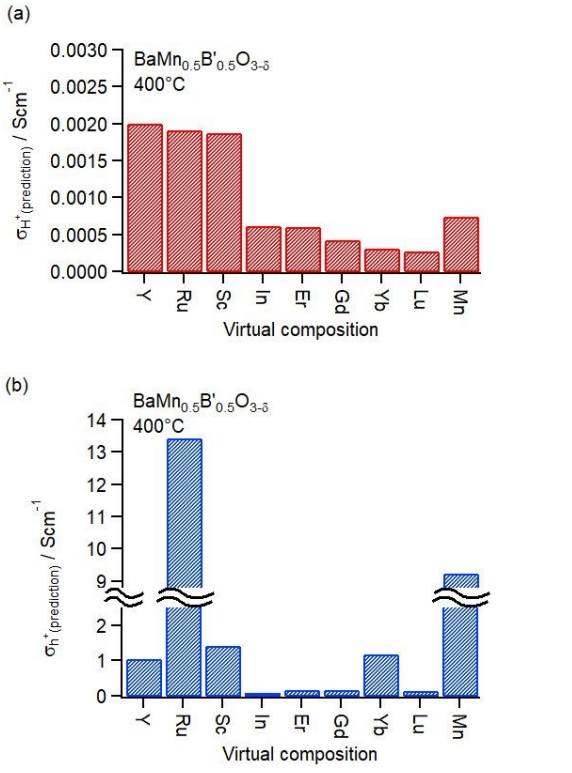

Figure 8 Prediction of the proton and hole conductivities of $BaMn_{0.5}M_{0.5}O_3$ (M = Gd, Y, Yb, In, Sc). (a) Proton and (b) hole conductivity

View Article Online
DOI: 10.1039/D6MA00607H

conductivities using machine learning yielded different accuracies, making direct comparison of their magnitudes difficult. Therefore, the presence or absence of proton conductivity was experimentally verified for $BaMn_{(1-x)/2}Y_{(1-x)/2}InxO_3$ (x = 0.1, 0.3, 0.5, 0.7).

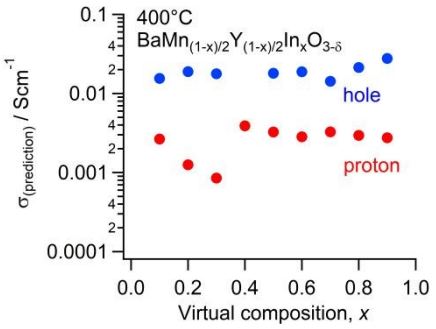

Figure 9 Prediction of proton and hole conductivity for $BaMn_{(1-x)/2}Y_{(1-x)/2}In_xO_3$

Verification of the recommended material The synthesis of $BaMn_{(1-x)/2}Y_{(1-x)/2}In_xO_3$ (x = 0.1, 0.3, 0.5, 0.7), recommended by machine learning, was conductedusing the chemical solution method. X-ray diffraction (XRD; MiniFlex600; Rigaku) using Cu-Kα1 radiation showed that $BaMn_{(1-x)/2}Y_{(1-x)/2}In_xO_3$ (x = 0.2, 0.5, 0.7) was single-phase. At x = 0.1, the sample became multi-phase, with a $Ba_6Y_{1.46}Mn_{4.54}O_{16.13}$ (ICSD184711) phase observed in addition to the perovskite phase (Figure S2(a)). The peak intensity at 36.6° decreased with increasing In content, indicating a transformation of the crystal structure from cubic perovskite to brownmillerite. The lattice constant increased with increasing In content, and heat treatment in a water vapor-containing atmosphere increased the lattice constant (Figure S2(b)). This is thought to be due to chemical expansion caused by crystal hydration.

To confirm the presence or absence of proton conductivity in $BaMn_{(1-x)/2}Y_{(1-x)/2}In_xO_3$ (x = 0.1, 0.3, 0.5, 0.7), the isotope effect (proton–deuterium substitution) on electrical conductivity was examined in the temperature range of 300°C–800°C. The temperature dependence of the electrical conductivity significantly varied with In concentration (Figure 10(a)). Furthermore, the isotope effect became distinctly observable with increasing In concentration, indicating a shift in the dominant charge carrier from other conductive species to protons (Figure 10(b)). At low In concentrations, the activation energy for electrical conductivity was 0.86 eV (x = 0.1), and the isotope effect was not observed. As the In concentration increased, the activation energy for electrical conductivity at low temperatures decreased (0.43 eV, *x = 0.5*), and the isotope effect was observed.

Proton conductivity can be roughly estimated from the ratio of the isotope effect to the electrical conductivity.

If electrical conductivity consists of proton and other conduction, such as holes, the ratio of conductivities in the isotope effect is expressed as follows:

$$r_{(H_2O/D_2O)} = \frac{\sigma_{\text{total, } H_2O}}{\sigma_{\text{total, } D_2O}} = \frac{\sigma_{\text{proton}} + \sigma_{\text{other}}}{\sigma_{\text{deuteron}} + \sigma_{\text{other}}} . \quad (2)$$

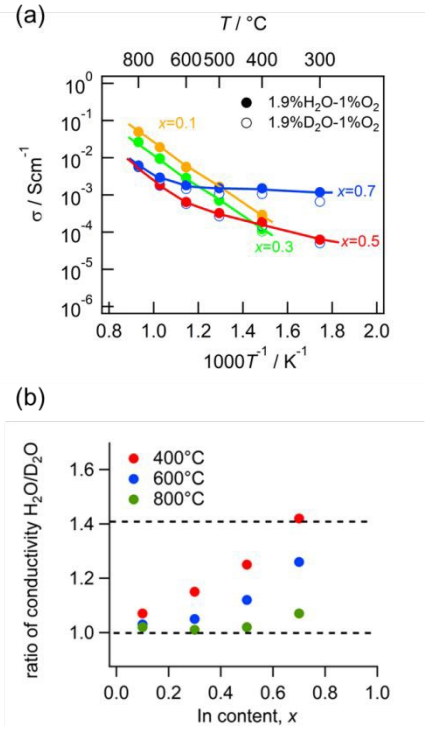

Figure 10 Conductivity and isotope effect of $BaMn_{(1-x)/2}Y_{(1-x)/2}In_xO_3$. (a) Temperature dependence of conductivity, and (b) ratio of conductivity under an H_2O/D_2O atmosphere

Here, $r_{(H_2O/D_2O)}$ is the ratio of the conductivity under H_2O to the conductivity under D_2O.

If proton migration is rate-limited to hopping between oxygen ions, diffusivity is inversely proportional to the square root of the proton mass. Since the square root of the mass ratio of deuteron to proton is expected to be 1.41 from the classical oscillation model[26], this ratio, Eq. (3), indicates that the major carrier species are protons.

$$\frac{\sigma_{\text{proton}}}{\sigma_{\text{deuteron}}} = 1.41 \quad (3)$$

Therefore, proton conductivity can be expressed using the following equation:

$$\sigma_{\text{proton}} = \frac{1.41(r-1)}{0.41r}\sigma_{\text{total, } H_2O} . \quad (4)$$

The proton conductivity required here is a rough estimate; if the ratio of the conductivities exceeds 1.41 due to the difference in

View Article Online
DOI: 10.1039/D6MA00607H

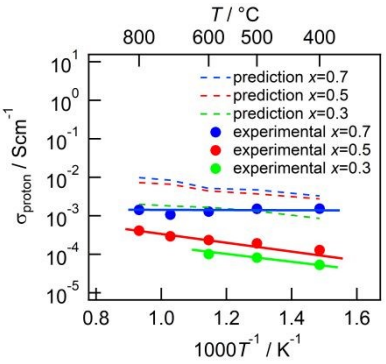

Figure 11 Comparison of measured and predicted proton conductivity values

zero-point motion energy between protons and deuterons, the estimate will be off, but even in the worst case, the error is expected to be around 30%.

The proton conductivities estimated using Eq. (4) were lower than the predicted values (Figure 11). This is thought to be influenced by issues with the prediction accuracy of the machine learning model. On the other hand, the sequence of proton conductivity based on composition was consistent. Proton conductivity is expressed as the product of the proton concentration and the diffusion coefficient. Previous studies have shown that the proton concentration can be predicted with high accuracy[24], and the discrepancy between the predictions and the measured values observed in this study is thought to be due to a lack of descriptors representing the diffusion coefficient. Recent studies have revealed that the diffusion coefficient is influenced not only by the type and amount of dopant elements but also by local structure[29]. Although this prediction model incorporates average structural information such as the tolerance factor, it does not include local structural information—such as oxygen octahedral distortion—as features; therefore, it is thought that the diffusion coefficient and, consequently, the proton conductivity cannot be accurately predicted.

X-ray photoelectron spectroscopy (XPS; ULTRA2; Kratos Analytical) indicated that Mn ions primarily exist in the +4 oxidation state and In ions in the +3 oxidation state (Figure S3 (a) and (b)). Considering the defects in $BaMn_{(1-x)/2}Y_{(1-x)/2}In_xO_3$, it is thought that Y or In is doped into $BaMnO_3$ as acceptors of oxide ion vacancies.

$$[\mathrm{In}'_{\mathrm{Mn}}]+[\mathrm{Y}'_{\mathrm{Mn}}]=[V_{\mathrm{O}}^{\bullet\bullet}] \quad (5)$$

It is believed that protons dissolve into the crystal via these oxide ion vacancies, thereby exhibiting proton conductivity, according to the following equation:

$$\mathrm{H_2O}+V_{\mathrm{O}}^{\bullet\bullet}+\mathrm{O}_{\mathrm{O}}^{\times}=2\mathrm{OH}_{\mathrm{O}}^{\bullet} \quad . \quad (6)$$

The XRD pattern (Figure S2(a)) indicates a transition to a brownmillerite due to an increase in In content. This is suggestive of the formation of a large number of oxide ion vacancies. Proton conduction is exhibited through the introduction of protons via these oxide ion vacancies. The increased proton concentration may explain the observed increase in proton conductivity with rising In concentration.

The proton conductivity of $BaMn_{0.15}Y_{0.15}In_{0.7}O_3$ developed in this study was 0.0012 S cm^{-1} at 300°C. The proton conductivity of $BaZr_{0.8}Y_{0.2}O_{3-\delta}$, a common proton conductor, is 0.0034 S cm^{-1} at 300°C[27]. Recently, the proton conductivities of $BaZr_{0.4}Sc_{0.6}O_{3-\delta}$, $BaMo_{0.2}Sc_{0.8}O_{3-\delta}$[28], and $BaSn_{0.3}Sc_{0.7}O_{3-\delta}$[29] doped with high concentrations of Sc have been reported as 0.0036 S/cm, 0.0092 S/cm, and 0.011 S/cm, respectively, at 300°C. Compared to these materials, the value obtained in this study is approximately a third lower. The proton conductivity achieved in this study is likely due to Y and In functioning as dopants, resulting in a high concentration of dissolved protons. On the other hand, the material composed of Mn, Y, and In exhibited lower mobility than the previously reported system with high-concentration Sc doping and did not demonstrate higher proton conductivity.

Experimental

Sample synthesis

$BaMn_{(1-x)/2}Y_{(1-x)/2}In_xO_3$ (x = 0.1, 0.3, 0.5, 0.7) were synthesized using a chemical solution method with nitrate as the starting material[19]. $Ba(NO_3)_2$ (99.9%; Wako Pure Chemical Industries, Ltd.), $Mn(NO_3)_3{\cdot}6.05H_2O$ (99.9%; Wako Pure Chemical Industries, Ltd.), $Y(NO_3)_3{\cdot}6.23H_2O$ (99.9%; Wako Pure Chemical Industries, Ltd.), $In(NO_3)_{33}{\cdot}3.29H_2O$ (98.0%; Kojundo Chemical Lab. Co., Ltd.), distilled water, citric acid (Wako Pure Chemical Industries, Ltd.), and EDTA (99.0%; Wako Pure Chemical Industries, Ltd.) were mixed while maintaining a pH of 10 by adding aqueous ammonia. The mixture was heated to 573 K. The obtained precursor was then calcined in air for 10 h at 900°C. The powder was milled and pressed into pellets at 250 MPa using CIP. The pellets were sintered at 1400°C (x = 0.5, 0.7) and 1400°C (x = 0.1, 0.30) for 5 h in air. The compacted density was 89%–95% (Figure S4).

Sample characterization

The crystal structure and lattice constant of the sample were confirmed by XRD. The as-sintered sample and the sample after impedance measurement under an oxidizing atmosphere (1.9%H_2O-1%O_2-Ar) were measured at room temperature. In addition, XPS was performed on the powder sample. The powder samples were prepared by crushing the disk samples after impedance measurements, assuming that the valence of Mn would freeze at 300°C during the experiment.

Impedance analysis

The electrical conductivity was measured using a two-probe AC technique. The shape of the sample was a pellet (ϕ: 1.3–1.4

View Article Online
DOI: 10.1039/D6MA00607H

mm, l: 0.5 mm). The complex impedance was measured in the 4–8 MHz frequency range using an LCR meter (IM2526; HIOKI). For the electrical measurements, silver paste (MH-1069P; TANAKA PRECIOUS METAL TECHNOLOGIES Co., Ltd.) was deposited on both surfaces of the pellet. Each sample was then sandwiched between silver mesh current collectors and annealed at 900°C for 1 hour under air. The samples were held at 800°C for a few hours to equilibrate under 1.9%H_2O-1%O_2-Ar. The conductivity was measured during cooling from 800°C to 300°C.

To confirm the proton/deuteron isotope effect on the conductivity, the conductivity was measured during cooling from 800°C to 300°C and recorded at several temperatures with an equilibration state under 1.9%H_2O (or 1.9%D_2O)-1%O_2. The Nyquist plot of the impedance spectra displayed well-resolved arcs (Figure S5).

Conclusions

This study determined that $BaMn_{(1-x)/2}Y_{(1-x)/2}In_xO_3$ exhibits high proton conductivity at low temperatures, based on machine learning predictions of proton and hole conductivities. The machine learning predictions suggested that Mn is the most suitable element among Co, Mn, Ni, and Fe as the host element for proton conductors in the B site. Furthermore, it was predicted that adding Y would enhance proton conductivity, while adding In would suppress hole conductivity.

$BaMn_{0.15}Y_{0.15}In_{0.7}O_3$ exhibited a proton conductivity of 0.0012 S cm^{-1} at 300°C. As the In concentration decreased in $BaMn_{(1-x)/2}Y_{(1-x)/2}In_xO_3$, proton conductivity decreased, and it was found that it becomes a charge carrier dominated by hole conduction.

The predicted proton conductivity values exceeded the measured values, indicating that the prediction accuracy for both proton and hole conductivities is an issue. Although the current prediction model can identify new materials with proton conductivity, it is difficult to find materials with high proton conductivity using this machine learning model. Since proton and hole conductivities are predicted separately, the model cannot accurately predict the mixed conductivity of protons and holes. Consequently, the developed prediction model cannot be used for material development, i.e., for electrode materials. Therefore, it is necessary to train the model to learn correlations between proton and hole conductivities, which requires improving the machine learning model.

Author contributions

Yuji Okuyama: conceptualization, methodology, validation, formal analysis, investigation, writing–original draft, review and editing, and supervision. Renta Kawakami: investigation and formal analysis. Kota Douzono: investigation.

Conflicts of interest

There are no conflicts to declare.

Data availability

The data that support the findings of this study are available from the corresponding author, [YO], upon reasonable request.

Acknowledgements

This work was partially supported by the NEDO project (JPNP20003) and the GteX program (JPMJGX23H).

References

1 T. Takahashi and H. Iwahara, *Rev. Chim. Miner.*, 1980, **17**, 243–253.
2 H. Iwahara, H. Uchida, K. Ono and K. Ogaki, *J. Electrochem. Soc.*, 1988, **135**, 529–533.
3 K. D. Kreuer, *Annu. Rev. Mater. Res.*, 2003, **33**, 333–359.
4 K. Tsujikawa, J. Hyodo, S. Fujii *et al.*, *Nat. Mater.*, 2025, **24**, 1949–1956.
5 H. Iwahara, T. Esaka, H. Uchida and N. Maeda, *Solid State Ionics*, 1981, **3–4**, 359–363.
6 A. Mitsui, M. Miyayama, H. Yanagida, Proceeding of the 3rd Meeting on Chemical Sensor, 1984 43, Oct. 9-10, Tokyo, Japan.
7 H. Iwahara, H. Uchida, K. Ono and K. Ogaki, *J. Electrochem. Soc.*, 1988, **135**, 529–533.
8 H. Iwahara, T. Yajima, T. Hibino, K. Ozaki and H. Suzuki, *Solid State Ionics*, 1993, **61**, 65–69.
9 T. Yajima, H. Kazeoka, T. Yogo and H. Iwahara, *Solid State Ionics*, 1991, **47**, 271–275.
10 Y. Larring and T. Norby, *Solid State Ionics*, 1994, **70**, 305–310.
11 D. Lybye and N. Bonanos, *Solid State Ionics*, 1999, **125**, 339–344.
12 H. Fujita, Y. Katayama, T. Shimura and H. Iwahara, *J. Electrochem.*, 1998, **2**, 119.
13 Y. Okuyama, T. Kozai, T. Sakai, M. Matsuka and H. Matsumoto, *Electrochim. Acta*, 2013, **95**, 54–59.
14 W.-K. Lee and A. S. Nowick, *Solid State Ionics*, 1986, **18–19**, 989–993.
15 T. Omata and S. Otsuka-Yao-Matsuo, *J. Electrochem. Soc.*, 2001, **148**, E252–E261.
16 N. Kitamura, K. Amezawa, Y. Tomii and N. Yamamoto, *Solid State Ionics*, 2003, **162**, 161–165.
17 K. Amezawa, Y. Tomii and N. Yamamoto, *Solid State Ionics*, 2003, **162–163**, 175–180.
18 R. Haugsrud and T. Norby, *Solid State Ionics*, 2006, **177**, 1129–1135.
19 T. Norby, O. Dyrlie and P. Kofstad, *J. Am. Ceram. Soc.*, 1992, **75**, 1176–1181.
20 T. Norby and P. Kofstad, *High Temp. High Press.*, 1988, **20**, 345–360.
21 Y. Okuyama, N. Kurita and N. Fukatsu, *Solid State Ionics*, 2009, **180**, 175–182.
22 Y. Okuyama, N. Kurita and N. Fukatsu, *Ionics*, 2009, **15**, 43–48.
23 K. Ishibashi, Y. Okuyama, N. Kurita and N. Fukatsu, *J. Jpn. Inst. Met.*, 2011, **75**, 229–234.
24 J. Hyodo, K. Tsujikawa, M. Shiga, Y. Okuyama and Y. Yamazaki, *ACS Energy Lett.*, 2021, **6**, 2985–2992.
25 K. Nomura, H. Shimada, Y. Yamaguchi, H. Sumi, Y. Mizutani, Y. Okuyama and W. Shin, *Ceram. Int.*, 2023, **49**, 5058–5065.
26 A. S. Nowick and A. V. Vaysleyb, *Solid State Ionics*, 1997, **97**, 17–26.

View Article Online
DOI: 10.1039/D6MA00607H

27 T. Kuroha, Y. Niina, M. Shudo, G. Sakai, N. Matsunaga, T. Goto, K. Yamauchi, Y. Mikami and Y. Okuyama, *J. Power Sources*, 2021, **506**, 230134.
28 K. Saito and M. Yashima, *Nat. Commun.*, 2023, **14**, 7466.
29 K. Tsujikawa, J. Hyodo, S. Fujii, K. Takahashi, Y. Tomita, N. Shi, Y. Murakami, S. Kasamatsu and Y. Yamazaki, *Nat. Mater.*, 2025, **24**, 1949–1956.

View Article Online
DOI: 10.1039/D6MA00607H

Data availability statement

The data that support the findings of this study are available from the corresponding author, [YO], upon reasonable request.